Angular anisotropy of electron energy distributions in inductively coupled plasmas

Alex V. Vasenkov[a] and Mark J. Kushner[b]
Department of Electrical and Computer Engineering, University of Illinois, 1406 West Green Street, Urbana, Illinois 61801

(Received 2 June 2003; accepted 6 August 2003)

The noncollisional electron transport that is typical of low-pressure (<10 mTorr) and low-frequency (<10 MHz) inductively coupled plasmas (ICPs) has the potential to produce highly anisotropic angle-dependent electron energy distributions (AEEDs). The properties of AEEDs in axially symmetric ICPs were investigated using a Monte Carlo simulation (MCS) embedded in a two-dimensional plasma equipment model. A method was developed to directly compute the coefficients for a Legendre polynomial expansion of the angular dependence of the distributions during advancement of the trajectories of pseudoelectrons in the MCS. We found significant anisotropy in the AEEDs for transport in the azimuthal–radial plane for a wide range of pressures and frequencies, and attributed this behavior to the superposition of both linear and nonlinear forces. The angular anisotropy of AEEDs in the radial–axial plane in the bulk plasma was found to be significant only when the skin layer was anomalous and nonlinear Lorentz forces are large. [DOI: 10.1063/1.1614428]

I. INTRODUCTION

Low- and intermediate-pressure inductively coupled plasmas (ICPs) are currently used for etching and deposition in microelectronics fabrication,[1–3] fluorescent lighting,[4,5] and for the growth of materials such as aligned carbon nanotubes.[6] Power in ICPs is largely transferred from the radio-frequency (rf) electric fields to electrons within the electromagnetic skin layer. Many experimental and theoretical studies of this region have shown that the electron energy distributions (EEDs) are generally non-Maxwellian as a result of nonequilibrium transport of electrons.[7–10] At the same time, little is known about the angular dependence of the EEDs in and near the skin layer, particularly, when the skin layer is anomalous.[11] This is partly a consequence of the difficulty of making electric probe measurements of angle-dependent electron energy distributions (AEEDs).[12]

The angular anisotropy of the AEED in ICPs is often assumed to be small so that a two-term spherical harmonic expansion can be used in the direct solution of Boltzmann's equation.[8,13,14] This assumption works well for high-pressure or highly collisional plasmas, and for conditions where inelastic collision frequencies are small compared to elastic collision frequencies. These conditions may not be met even in swarm experiments.[15] As a result, the two-term approximation becomes increasingly less applicable as the pressure decreases to the regime of interest for microelectronics fabrication (<10 mTorr). For example, measurements of electron drift velocities in the skin layer of an ICP reactor at 10 and 50 mTorr by Meyer *et al.* were found to be comparable to the local electron thermal velocities, which suggests that the AEEDs were considerably anisotropic.[16] Kolobov *et al.* computationally investigated the angular distribution of electrons in an ICP having a coaxial solenoidal coil.[17] They found that the angular distribution of electrons with energies above the plasma potential was anisotropic in the radial–axial (rz) plane and that this anisotropy depends on the radial position (distance from the coil).

In this article, we report on results from a computational investigation of the angular anisotropy of AEEDs in low-pressure ICPs sustained in Ar and Ar/C_4F_8. Legendre polynomial coefficients describing the angular dependence of kinetically derived AEEDs are derived using sampling techniques in a Monte Carlo simulation. The test reactor is cylindrically symmetric with a flat coil having antenna current oscillating in the azimuthal direction. ("θr" refers the azimuthal–radial plane. "rz" refers to the radial–axial plane.) We found that there is significant angular anisotropy in the AEEDs in the θr plane over a wide range of pressures (1–50 mTorr) and frequencies (1.13–13.56 MHz). Angular anisotropy in the rz plane occurs in the skin layer for most conditions and in the bulk plasma only when the skin layer is anomalous. We attributed these two types of anisotropy to electron acceleration by linear electrodynamic and nonlinear third-order forces, and noncollisional electron transport due to nonlinear Lorentz forces. The model is described in Sec. II and the results of our investigation are discussed in Sec. III. Concluding remarks are in Sec. IV.

II. DESCRIPTION OF THE MODEL

The model employed in this study is the Hybrid Plasma Equipment Model (HPEM) described in detail in Ref. 10, and references therein. The model consists of three major

[a]Present address: CFD Research Corp., 215 Wynn Drive, Huntsville, AL 35805; electronic mail: avv@cfdrc.com
[b]Author to whom correspondence should be addressed: electronic mail: mjk@uiuc.edu

modules. The electromagnetics module (EMM) is used to solve Maxwell's equations for rf magnetic and electric fields. These fields are than used in the electron energy transport module (EETM) where electron transport coefficients and source functions are calculated using the electron Monte Carlo simulation (EMCS). The EMCS is strongly coupled to the EMM as electron currents used in solution of Maxwell's equations are directly calculated in this module. In large part due to this coupling, the EMCS addresses noncollisional heating, nonlinear electron dynamics, and warm plasma effects, which are significant at low pressure when the skin layer is anomalous.[9,14,18] Results from the EETM are transferred to the fluid-chemical kinetics module (FKM), which solves the continuity, momentum, and energy equations for densities, momenta, and temperatures of neutrals and charged species, and Poisson's equation for the electrostatic potential. The sheath at the walls was not explicitly resolved in the solution of Poisson's equation as the sheath width was considerably smaller than the size of the computational mesh and the skin depth for the pressures and frequencies of interest. These modules are iterated until a converged solution is obtained. Although the EMM and FKM are two-dimensional, the EMCS is fully three-dimensional, and so resolves transport in the θr and rz planes.

The time-averaged spatially dependent AEEDs are obtained by recording statistics on the energy, location and direction of electron pseudoparticles while their trajectories are advanced in the EMCS. The methods of advancing the pseudoparticle trajectories (employing electron–neutral, electron–ion, and electron–electron collisions), and the manner of recording energies as a function of position, are described in Ref. 10. The angular dependence of the AEEDs obtained from the EMCS are quantified here using a Legendre polynomial expansion. The full anisotropic character of the AEEDs is directly available from the EMCS and could, in principle, be recorded by binning the pseudoparticles in angle as well as energy. Based on past experience in deriving the harmonic time dependence of excitation rates in similar discharges,[19] we chose the expansion approach as being more robust against statistical noise and more amenable to analysis.

In this method, the AEEDs in the θr or rz plane, f, are given by

$$f(\epsilon,\mathbf{r},\phi)=\sum_{\ell} a_{\ell}(\epsilon,\mathbf{r})P_{\ell}(\cos\phi), \tag{1}$$

where ϵ is the electron energy, $\mathbf{r}$ is the spatial location, P_{ℓ} is the ℓth Legendre polynomial, and a_l is the ℓth Legendre polynomial coefficient. ϕ is the angle of the electron trajectory with respect to a reference direction, ϕ_0. In the rz plane, ϕ_0 is aligned with the z axis pointing up from the substrate to the coils. In the θr plane, ϕ_0 is aligned with the local azimuthal tangent in the direction of the azimuthal electric field. For brevity in the following, $\mu=\cos(\phi)$.

The raw statistics from which a_{ℓ} are computed, $A_{\ell}(\epsilon,\mathbf{r})$, are updated as electron trajectories and are advanced in the EMCS. After each update of the trajectories of the pseudoparticles,

$$A_l(\epsilon_i,\mathbf{r}_k)\rightarrow A_l(\epsilon_i,\mathbf{r}_k)+\sum_j \Delta\Phi_{ikj} \times\sum_n\left\{\frac{2l+1}{2}\delta[(\mu_n\pm\tfrac{1}{2}\Delta\mu_n)-\mu_j]P_l(\mu_n)\right\}, \tag{2}$$

where

$$\Delta\Phi_{ikj}=w_j\Delta t_j\delta[(\epsilon_i\pm\tfrac{1}{2}\Delta\epsilon_i)-\epsilon_j] \times\sum_m \alpha_m\delta[(\mathbf{r}_{m+k}\pm\tfrac{1}{2}\Delta\mathbf{r}_{m+k})-\mathbf{r}_j].$$

ϵ_i and $\mathbf{r}_k$ are the energy and location of the ith energy bin and kth spatial mesh cell having widths $\Delta\epsilon_i$ and $\Delta\mathbf{r}_k$. The summations are over j pseudoparticles and n bins discretizing angles. The δ function isolates the bin where $\mu_n-\frac{1}{2}\Delta\mu_n\leqslant\mu_j\leqslant\mu_n+\frac{1}{2}\Delta\mu_n$. $\Delta\Phi_{ikj}$ is a coefficient which accounts for binning the particle j in energy and position. w_j is a pseudoparticle-dependent weighting, which accounts for the number of electrons the pseudoparticle represents, and Δt_j is the previous time step. α_m is a weighting to account for finite-sized-particle distributions. At the end of given iteration through the EMCS, the coefficients, $a_l(\epsilon_i,\mathbf{r}_k)$ are obtained from the raw statistics $A_l(\epsilon_i,\mathbf{r}_k)$ as

$$a_l(\epsilon_i,\mathbf{r}_k)=A_l(\epsilon_i,\mathbf{r}_k)\Bigg/\left[\sum_i A_0(\epsilon_i,\mathbf{r}_k)\int_{-1}^{1}P_0\,d\mu\right]. \tag{3}$$

Here, $2a_0(\epsilon_i,\mathbf{r}_k)$ is equivalent to the angle-averaged AEED.

No special boundary conditions are applied to electron motion in the EMCS as the kinetic dynamics of the electrons are followed through the presheath and sheath to the wall; and removed from the simulation if they strike the walls. Although the sheath width is not fully resolved, the electron mean-free path exceeds both the sheath width and a numerical cell width. As such, energy is appropriately conserved for trajectories which pass through these regions, a condition which is enforced by dynamic choice of the integration time step and use of higher-order integration techniques.

III. COLLISIONAL, LINEAR, AND NONLINEAR EFFECTS ON AEEDS IN ICPS

A schematic of the reactor used in this study is shown in Fig. 1 and is patterned after that used by Standaert *et al.*[20] The ICP was produced in a cylindrically symmetric chamber (13 cm in radius and 12 cm tall) using a three-turn antenna set atop a quartz window 1 cm thick. Gas was injected through the inlet below the dielectric window and was pumped out from the bottom of the reactor. A metal ring was used to confine plasma. The electron-impact cross sections and heavy particle reaction rate coefficients used in this investigation for Ar are reported in Ref. 10. Those for Ar/C_4F_8 will be discussed in an upcoming publication.

A. Plasma properties, Legendre coefficients, and AEEDs

An antenna produces a rf magnetic field B_{rf} in the plane perpendicular to the θ axis as shown in Fig. 1. This rf magnetic field creates an inductively coupled azimuthally di-

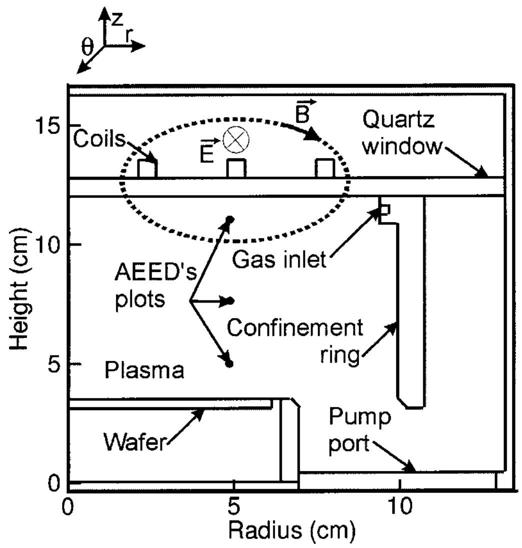

FIG. 1. Schematic of the cylindrically symmetric ICP reactor. The rf electric field has only a tangent component E_θ, whereas the rf magnetic field is dominantly radially directed.

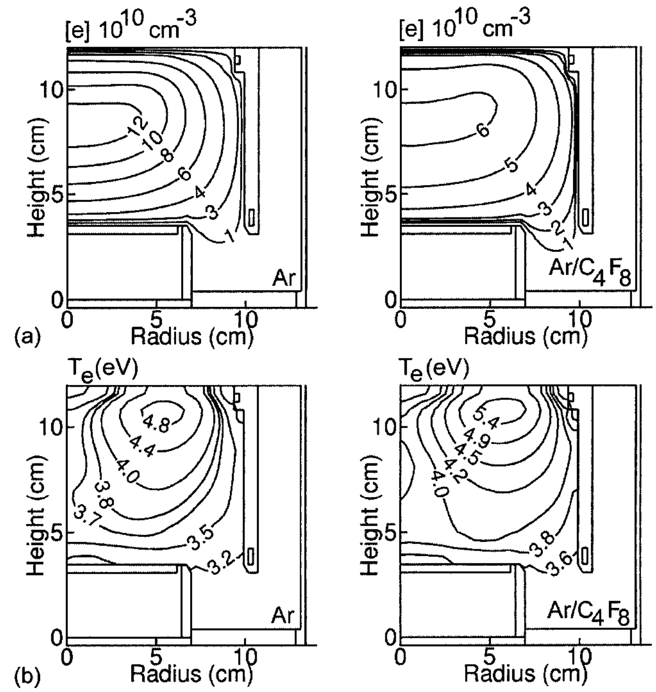

FIG. 2. Plasma parameters for the base case conditions (3 mTorr, 400 W, 3.39 MHz). (a) Electron density and (b) electron temperature for Ar and Ar/C_4F_8 mixtures. Electron density peaks in the middle of the reactor near the peak of plasma potential, whereas the electron temperature has a maximum at the edge of skin layer as a consequence of noncollisional heating.

rected electric field E_θ. There are at least five dominant forces that act upon electrons. The first is the electrodynamic force $-|q|E_\theta$, q is the electron charge, which accelerates electrons in the θr plane. The second is the electrostatic force $-|q|E_s$, which accelerates electrons in the rz plane towards the peak of the plasma potential in the middle of discharge. The third is the second-order nonlinear Lorentz force (NLF), $\mathbf{v}\times\mathbf{B}_{\mathrm{rf}}$, produced by the rf magnetic field. $\mathbf{B}_{\mathrm{rf}}$ is dominantly radially directed under the coils and $\mathbf{v}$ has a large azimuthal component due to acceleration by E_θ. The result is that the NLF produces acceleration axially downward for our geometry. Recently, Tasokoro *et al.* experimentally found evidence for a fourth force F_{sh} resulting from the superposition of the ambipolar electrostatic field and the rf magnetic field $\mathbf{F}_{\mathrm{sh}}\sim\mathbf{E}_s\times\mathbf{B}_{\mathrm{rf}}$.[21] This force is dominantly directed in the θ direction for our geometry. We found that there is fifth force acting on the electrons in the θr plane, which is commensurate with the linear electrodynamic force at low pressures and low frequencies. This force, $F_\theta^{(3)}$ is due to the rf electric and magnetic fields.

The electron density and temperature T_e are shown in Fig. 2 for the base case conditions (3 mTorr, 400 W, 3.39 MHz) for ICPs sustained in Ar and Ar/C_4F_8=70/30. The peak electron density, which results from the drift of thermal electrons towards the peak of the plasma potential, is $1.2\times10^{11}\,\mathrm{cm}^{-3}$ in Ar and $6\times10^{10}\,\mathrm{cm}^{-3}$ in Ar/C_4F_8. The peak plasma potential is 13.4 V in Ar and 13.0 V in Ar/C_4F_8. The lower electron density in Ar/C_4F_8 is due in large part to the higher rate of power dissipation per electron in the more collisional molecular gas mixture. T_e peaks at the edge of the skin depth, 4.8 eV in Ar and 5.4 eV in Ar/C_4F_8. Due to higher rates of loss by attachment to C_4F_8 and its fragments a higher T_e is required to sustain the plasma.

The first five expansion coefficients $a_\ell(\epsilon,r,z)$ for the angular anisotropy of the AEEDs in Ar and Ar/C_4F_8 are shown in Figs. 3 and 4 in the rz and θr planes for the base case conditions. Coefficients are given at a radius of 5 cm, which corresponds to the position of the maximum in E_θ, and for three heights. These heights, 11, 8, and 5 cm, are in the electromagnetic skin layer (about 2 cm thick for the base case conditions), bulk plasma, and near the substrate, respectively. (These locations are noted in Fig. 1.) The Legendre coefficients in Ar and Ar/C_4F_8 show similar trends, which are described as follows.

The expansion coefficients in the rz plane obtained using reference angle μ_0 aligned along the z axis are shown in Fig. 3. In the skin layer, a_0 significantly exceeds the other coefficients for energies below the plasma potential, implying that the AEED, involving electrons electrostatically trapped in the plasma, is nearly isotropic. The odd coefficient a_3 dominates and $a_3\approx a_0$ for energies >25–30 eV. Odd Legendre coefficients represent anisotropy in the forward direction, which in this case is aligned downward along the z axis. The large values of the odd coefficients imply that nearly all high-energy electrons are accelerated out of the skin layer into the bulk plasma by the NLF. In the bulk plasma, where the NLF is small and electrons experience a large number of electron–electron and electron–heavy particle collisions, a_1 and a_2 dominate, and a_3 is large only for energies above 30 eV. Near the substrate the coefficients are small at energies below the plasma potential, implying isotropic AEEDs. a_2 is relatively large at energies above 20 eV, producing an AEED stretched in both the $-v_z$ and $+v_z$ directions.

The first five expansion coefficients for AEEDs for Ar and Ar/C_4F_8 in the θr plane are shown in Fig. 4. The reference angle here is aligned along the θ axis or the local tangent. The even coefficients a_l dominate at all positions implying that the AEEDs are stretched in both the $+v_\theta$ and

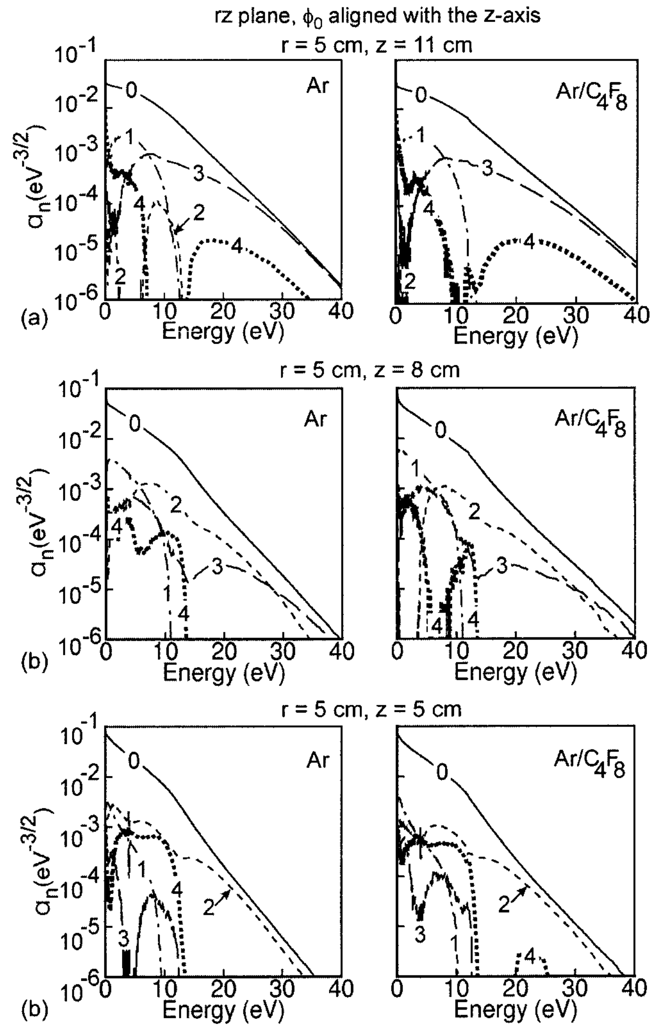

FIG. 3. First five Legendre expansion coefficients in the rz plane for the base case conditions at heights of (a) 11 cm, (b) 8 cm, and (c) 5 cm for Ar and Ar/C_4F_8 mixtures. Odd coefficients, implying anisotropy of the AEEDs in the $-v_z$ direction, dominate in the skin layer where the NLF peaks.

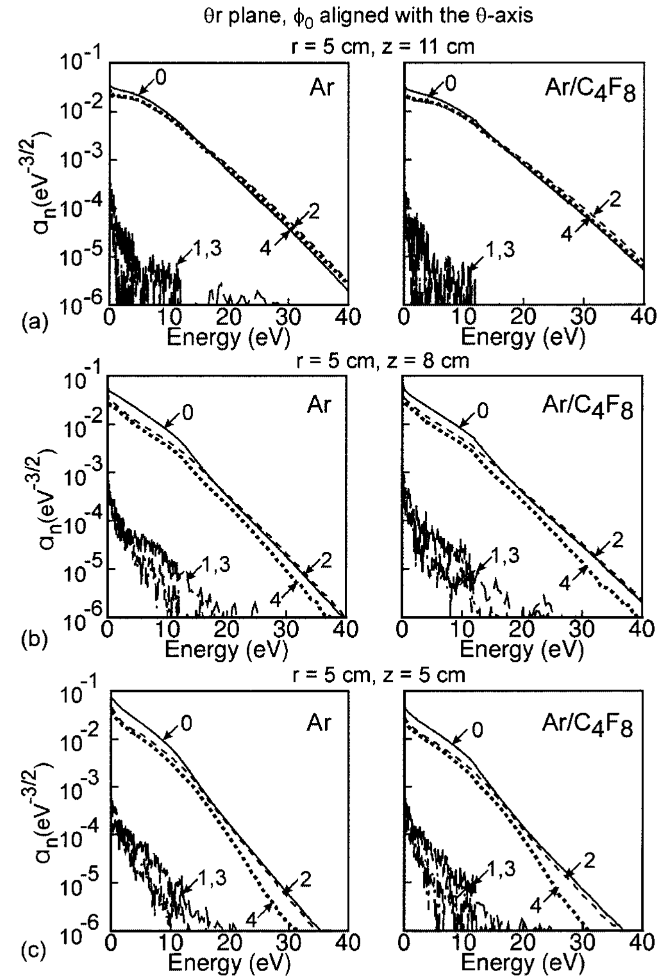

FIG. 4. First five Legendre expansion coefficients in the θr plane for the base case conditions at heights of (a) 11 cm, (b) 8 cm, and (c) 5 cm for Ar and Ar/C_4F_8 mixtures Large even coefficients imply that the AEEDs are stretched in the $-v_\theta$ and $+v_\theta$ directions.

$-v_\theta$ directions, especially for energies above the plasma potential. This azimuthal asymmetry in the AEED is intuitive as one would expect that the harmonic acceleration by E_θ would produce symmetric anisotropy, that is, even a_ℓ dominating. The even coefficients are particularly large in the skin layer where E_θ peaks. a_2 and a_4 are proportionally smaller in the bulk plasma and near the substrate due to electron–electron and electron–heavy particle collisions reducing the anisotropy.

The AEEDs in Ar and Ar/C_4F_8 as functions of the v_z and v_r, and v_θ and v_r velocity components are shown in Fig. 5 in the middle of skin layer for the base case conditions when seven Legendre expansion components are used. The angular distributions of electrons with energies below the plasma potential are nearly isotropic in the rz plane with a small shift in the $-v_z$ direction due to the drift of electrons towards the peak of the plasma potential. The anisotropy of the AEEDs in the $-v_z$ direction increases with energy in large part due to the NLF, which accelerates high-energy electrons out of the skin layer.

In contrast, the AEEDs obtained in the θr plane using the tangent as the reference direction are anisotropic at both low and high energies. At the beginning of a rf cycle, the skin layer is populated by only thermal electrons. As the rf cycle progresses, these low-energy electrons increase in energy and also accumulate anisotropy. The frequency of electron–electron and electron–heavy particle collisions is insufficient at these low pressures to randomize the angular distribution of these electrons. Consequently, the time-averaged AEEDs, which include electrons from different portions of the rf cycle, are anisotropic in all energy ranges.

The angular anisotropy in the low-energy part of AEEDs in the θr plane results in proportionally large θ-directed drift velocities in the skin layer. The average drift speed w_θ can be estimated as J_θ/en_e, where J_θ is the amplitude of current density in the θ direction and n_e is the electron density. For the base case conditions of 3 mTorr $w_\theta = 1.3\times 10^8$ cm/s. The drift velocity decreases with increasing pressure. For example, at 10 mTorr and 200 W, the maximum of drift velocity is $\approx 5.3\times 10^7$ cm/s. Meyer *et al.* measured $w_\theta \approx 5\times 10^7$ cm/s for similar conditions.[16]

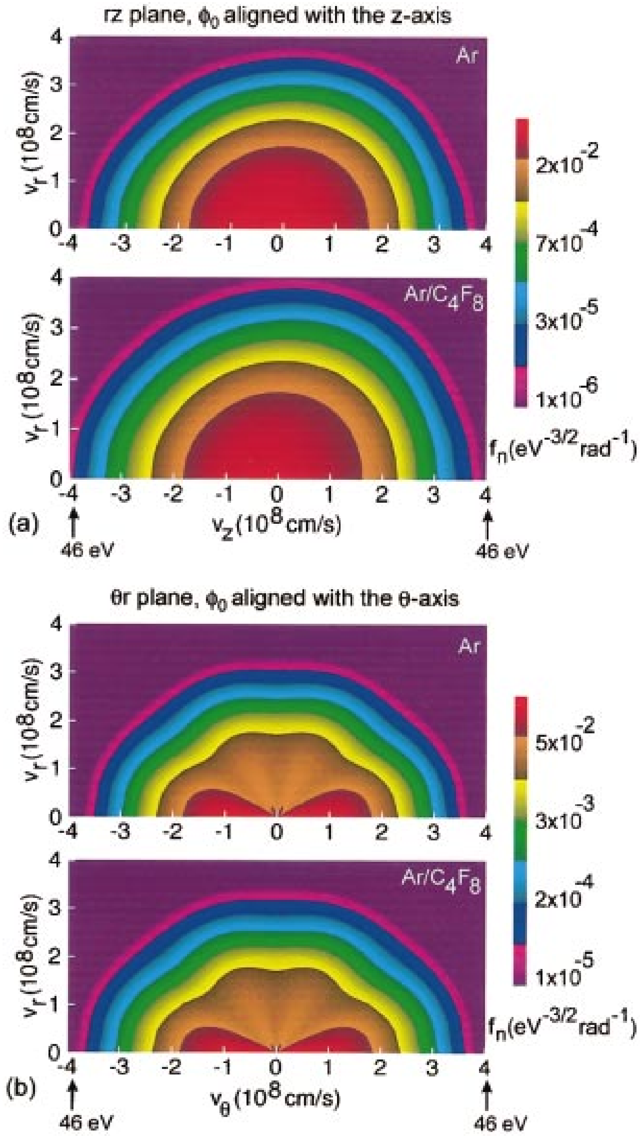

FIG. 5. (Color) AEEDs in the middle of the skin layer, $(r,z) = (5\text{ cm},11\text{ cm})$, in the (a) rz and (b) θr planes for the base case conditions for Ar and Ar/C_4F_8 mixtures. The anisotropy of the AEEDs increases with energy in the rz plane in large part due to the NLF. In contrast, the AEEDs in the θr plane are anisotropic at both low and high energies.

B. Linear and nonlinear forces in ICPs

The angular anisotropy of the AEEDs is attributed to the superposition of linear and nonlinear forces. The linear equation of motion involves the electrodynamic force accounting for electron acceleration in the v_θ direction and collisional damping[22]

$$\mathbf{F}_\theta^{(1)} = m\frac{d\mathbf{v}_\theta^{(1)}}{dt} = -|q|\mathbf{E}_\theta - m\mathbf{v}_\theta^{(1)}\nu_m, \tag{4}$$

where $E_\theta = E_\theta^0\cos(\omega t)$. This equation is valid for weakly ionized cold plasmas and does not account for the motion of thermal electrons, which is included in the model . $\mathbf{v}_\theta^{(1)}$, resulting from $F_\theta^{(1)}$, is then

$$\mathbf{v}_\theta^{(1)} = -\frac{|q|}{m}\frac{\mathbf{E}_\theta^0\cos(\omega t-\varphi)}{(\nu_m^2+\omega^2)^{1/2}}, \tag{5}$$

where $\varphi = \arctan(\omega/\nu_m)$. Without collisions the electron's acceleration due to $F_\theta^{(1)}$ produces only even coefficients in the θr plane as the electric field alternates between positive and negative values. Collisions randomizing the purely harmonic electron oscillations, yield the phase difference between $v_\theta^{(1)}$ and E_θ, and produce odd coefficients. These odd coefficients are rather small compared to the even coefficients at low pressure when electron motion is dominantly collisionless. They are proportionately larger at higher pressures when the collision frequency is larger.

Nonlinear forces, which are weak in the collision-dominated regime, can dominate under collisionless conditions (pressures <10 mTorr).[23] The equation of motion using a second-order nonlinear approximation is[23,24]

$$\mathbf{F}^{(2)} = m\frac{d\mathbf{v}^{(2)}}{dt} = -|q|\{(\mathbf{r}_\theta^{(1)}\boldsymbol{\nabla})\mathbf{E}_\theta - v_\theta^{(1)}B_r\mathbf{e}_z\}, \tag{6}$$

where we neglected the collisional damping term and ignored B_z compared to B_r. The second term on the right side of Eq. (6) is typically referred to as the NLF. The change in position $\mathbf{r}_\theta^{(1)}$ can be determined by integrating $\mathbf{v}_\theta^{(1)}$ with respect to time:

$$\mathbf{r}_\theta^{(1)} = -\frac{|q|}{m\omega}\frac{\mathbf{E}_\theta^0\cos(\omega t-\varphi)}{(\nu_m^2+\omega^2)^{1/2}}. \tag{7}$$

Substituting $\mathbf{r}_\theta^{(1)}$ and $\mathbf{v}_\theta^{(1)}$ in Eq. (6) with their expressions from Eqs. (5) and (7), using that

$$\frac{\partial E_\theta(r,z)}{\partial\theta} = 0, \tag{8}$$

and neglecting the term

$$(\mathbf{E}_\theta^0\boldsymbol{\nabla})\mathbf{E}_\theta^0 = -\frac{(E_\theta^0)^2}{r}\mathbf{e}_r, \tag{9}$$

as it is small everywhere except at the axis, one finds that the first term on the right side of Eq. (1) vanishes and the second term gives a force directed along the z axis:

$$\mathbf{F}_z^{(2)} = \frac{-q^2}{m(\nu_m^2+\omega^2)^{1/2}}\mathbf{e}_z E_\theta^0 B_r^0\sin(\omega t)\cos(\omega t-\varphi), \tag{10}$$

where we used that $B_r = B_r^0\sin(\omega t)$. In the collisionless case, $\nu_m \ll \omega$ and $\phi = \pi/2$, and Eq. (10) gives

$$F_z^{(2)} = \frac{-q^2}{2m\omega}[E_\theta^0B_r^0 - E_\theta^0B_r^0\cos(2\omega t)]. \tag{11}$$

The velocity $\mathbf{v}_z^{(2)}$ and change in position $\mathbf{r}_z^{(2)}$ are

$$\mathbf{v}_z^{(2)} = \frac{-q^2}{2m^2\omega^2}E_\theta^0B_r^0[\omega t - \sin(2\omega t)/2], \tag{12}$$

$$\mathbf{r}_z^{(2)} = \frac{-q^2}{4m^2\omega^3}E_\theta^0B_r^0[\omega^2t^2 + \cos(2\omega t)/2]. \tag{13}$$

$F_z^{(2)}$ consists of time-independent and time-dependent components. The first component accelerates electrons out of the skin layer and produces odd coefficients. The second component oscillating at the second harmonic produces time-averaged even coefficients. Owing to $F_z^{(2)}$ scaling as $1/\omega$, one should expect that the anisotropy of the AEEDs due to this force would decrease as the frequency increases.

The third-order equation of motion in the collisionless limit is[24]

$$\mathbf{F}^{(3)} = m\frac{d\mathbf{v}^{(3)}}{dt} = -|q|\{(\mathbf{r}_z^{(2)}\nabla)\mathbf{E}_\theta + v_z^{(2)}B_r\mathbf{e}_\theta\}. \tag{14}$$

Substituting $\mathbf{r}_2^{(2)}$ and $\mathbf{v}_2^{(2)}$ in Eq. (14) with their expressions from Eqs. (12) and (13), we find that the third-order force is directed along the tangent and is given by

$$\mathbf{F}_\theta^{(3)} = \frac{|q|^3}{4m^2\omega^2}\mathbf{e}_\theta E_\theta^0 [B_r^0]^2 [\omega^2 t^2 + 2\omega t + \cos(2\omega t)/2 - \sin(2\omega t)], \tag{15}$$

where we used that

$$B_r^0 = -\frac{1}{\omega}\frac{\partial E_\theta^0}{\partial z}. \tag{16}$$

Due to $F_\theta^{(3)}$ being inversely related to ω, $F_\theta^{(3)}$ is particularly large at low rf frequencies. The ratio of $F_\theta^{(3)}$ to $F_\theta^{(1)}$ in the collisionless regime can be estimated by averaging Eqs. (15) and (4) with $\nu_m = 0$ over half of the rf cycle when the electric field has a single sign. Using the base case plasma conditions and estimating B_r as 3 G at 13.56 MHz and 10 G at 1.13 MHz, one finds that $F_\theta^{(3)}/F_\theta^{(1)} \approx 5$ at 13.56 MHz and 10^2 at 1.13 MHz. Computational results presented below will support these estimates and show that the third-order nonlinear force can exceed the linear force $F_\theta^{(1)}$. As such, $F_\theta^{(3)}$ can be the dominant force on electrons in ICPs at low frequencies in the collisionless regime and an important mechanism for power deposition.

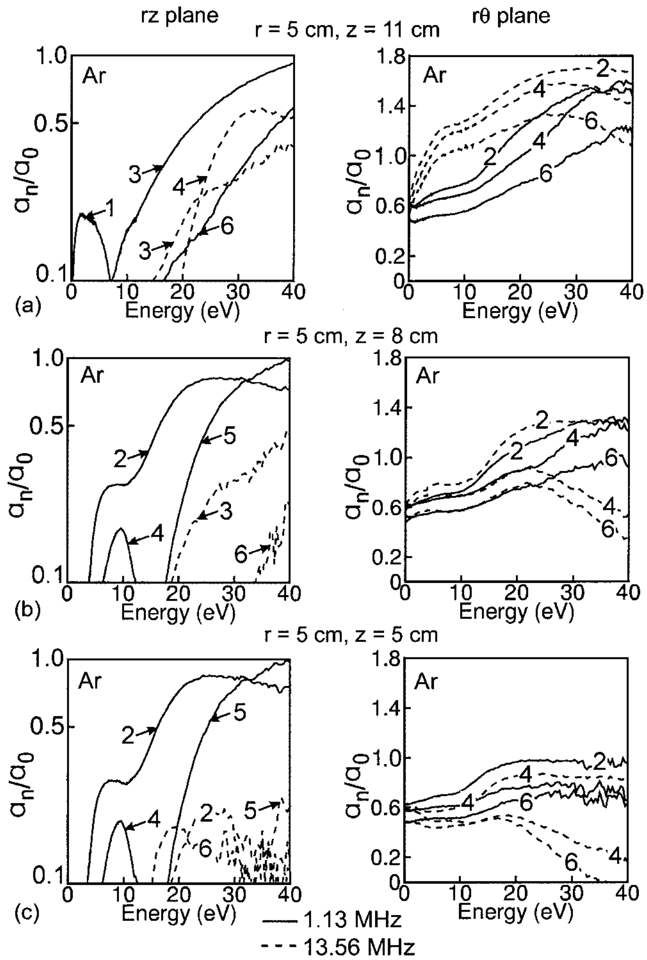

FIG. 6. a_n/a_0 for ICPs excited in Ar at 1.13 and 13.56 MHz in the rz and θr planes at heights of (a) 11 cm, (b) 8 cm, and (c) 5 cm. Odd coefficients increase with decreasing frequency in the rz plane as the NLF increases. The behavior of the coefficients in the θr plane is due to the superposition of linear and nonlinear effects.

C. Variations of AEEDs from collisionless to collisional conditions

The just described features of linear and nonlinear forces in ICPs are indicated by the ratios a_n/a_0 for different rf frequencies, but otherwise the base case conditions. These results, shown in Fig. 6, are for $r = 5$ cm for heights ranging from the skin layer (11 cm) to near the substrate (5 cm). In the rz plane, the contributions of higher-order terms at 1.13 MHz are larger than those at 13.56 MHz for all positions as $F_z^{(2)}$ increases with decreasing frequency. The odd coefficients are larger than even coefficients in the skin layer at 1.13 MHz and are commensurate with the even coefficients at 13.56 MHz. In the bulk plasma and close to the substrate, the even coefficients at 1.13 MHz are generally larger than the odd coefficients for energies below 25 eV, producing AEEDs elongated in the $+v_z$ and $-v_z$ directions and symmetric with respect to the r axis.

Only even coefficients are shown in the θr plane as the odd coefficients are small for both frequencies. The even coefficients are the largest in the skin layer, where $F_\theta^{(1)}$ and $F_\theta^{(3)}$ peak. Here, even coefficients for 13.56 MHz are larger than those at 1.13 MHz for energies below the plasma potential as a consequence of the increased value of the rf electric field and $F_\theta^{(1)}$ in the skin layer. In contrast, at energies above the plasma potential, even coefficients at 1.13 MHz are commensurate with those for 13.56 MHz, implying that the nonlinear forces $F_\theta^{(3)}$ acting on the high-energy electrons exceed the linear force $F_\theta^{(1)}$. In the bulk plasma and close to the substrate, the even coefficients for both frequencies are commensurate at energies below the plasma potential. At higher energies, a_2/a_0 is larger for 1.13 MHz, for which the nonlinear force $F_\theta^{(3)}$ is larger.

The ratios a_n/a_0 with and without B_{rf} for 1.13 MHz, but otherwise the base case conditions are shown in Fig. 7 for the rz and θr planes. Without B_{rf}, the NLF in the EMCS and $F_z^{(2)}$ in Eq. (11) are zero and the anisotropy of the AEEDs in the rz plane is due only to the thermal diffusion of electrons towards the peak in the plasma potential. In the middle of skin layer ($z = 5$ cm), the a_n/a_0 in the rz plane with B_{rf} for energies below 20 eV are larger than those obtained without B_{rf}. The coefficients are commensurate for energies above 20 eV. These results are a bit counterintuitive. The NLF should accelerate electrons out of the skin layer, and so odd coefficients with B_{rf} should dominate, which is what we observe at low energy. The large odd a_n/a_0 at higher energies without B_{rf} are likely a consequence of being close to the

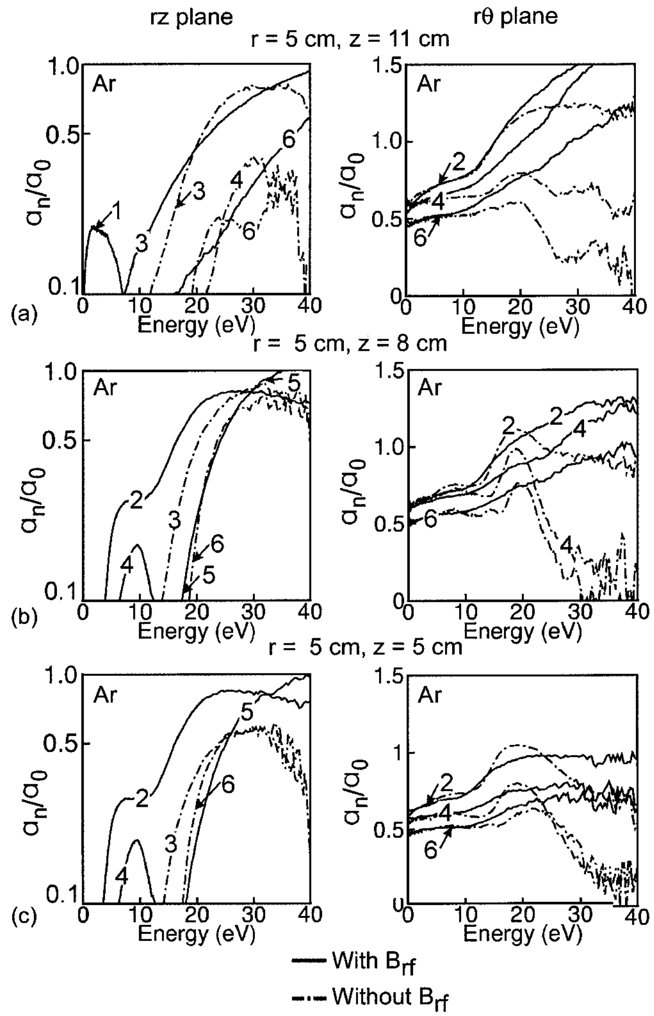

FIG. 7. a_n/a_0 with and without B_{rf} for ICPs in 1.13 MHz in Ar, but otherwise the base case conditions at heights of (a) 11 cm, (b) 8 cm, and (c) 5 cm. Without the NLF ($B_{rf}=0$) the anisotropy of the AEEDs in the rz plane is due to only the thermal motion of electrons. Coefficients with B_{rf} are similar to those without B_{rf} for energies below the plasma potential as they are determined by $F_\theta^{(1)}$, whereas coefficients at higher energies are significantly affected by B_{rf} as $F_\theta^{(3)}$ is directly proportional to B_{rf}.

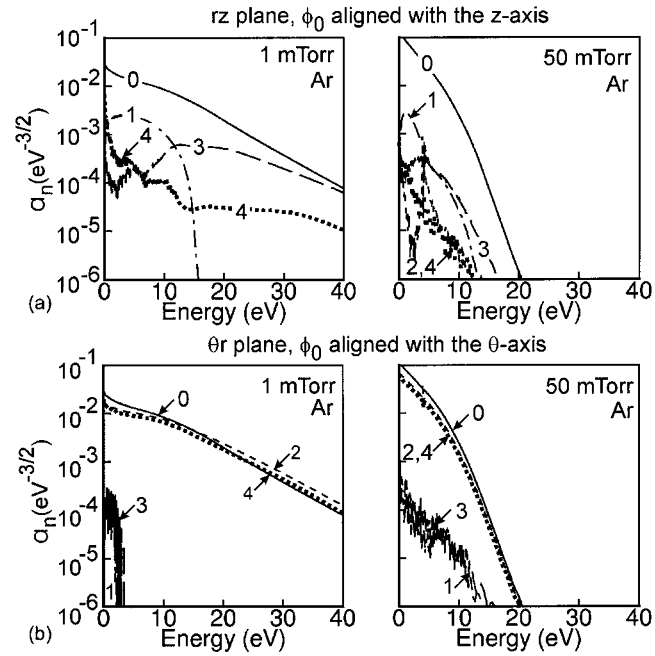

FIG. 8. a_n/a_0 at pressures of 1 and 50 mTorr in the middle of skin layer, $(r,z)=(5\text{ cm},11\text{ cm})$, for otherwise the base case conditions in the (a) rz and (b) θr planes. High-order coefficients in the rz plane large only at low pressure when the skin layer is anomalous. Even coefficients in the θr plane are large for a wide range of pressures as they are determined by the superposition of linear and nonlinear effects.

boundary of the plasma. High-energy electrons (above the plasma potential), moving vertically upwards, which would contribute to even a_n/a_0, are lost from the plasma leaving only those directed downward to contribute to odd a_n/a_0. In the middle of the plasma and near the substrate ($z=8$ and 5 cm) the lack of significant a_n/a_0 at low energies implies that without B_{rf} the AEEDs are fairly isotropic. Any directionality at these energies is due to residual effects of the NLF, which accelerate electrons out of the skin layer.

The anisotropy in the θr plane is determined by the superposition of the linear $F_\theta^{(1)}$ and nonlinear force $F_\theta^{(3)}$ given by Eqs. (4) and (15), respectively. $F_\theta^{(1)}$ is not affected by B_{rf}, whereas $F_\theta^{(3)}$ is directly proportional to B_{rf}. Consequently, a_n/a_0 with B_{rf} are similar to those without B_{rf} for energies below the plasma potential as electrons with these energies are electrostatically trapped in the plasma, and the anisotropy of their distribution is determined by $F_\theta^{(1)}$. Above the plasma potential, the coefficients with B_{rf} are significantly larger than those without B_{rf}, implying that the anisotropy of AEEDs at high energies is determined by $F_\theta^{(3)}$.

The differences in Legendre coefficients with and without B_{rf} could be in part due to the force $\mathbf{F}_{sh}\sim\mathbf{E}_s\times B_{rf}$ reported by Tasokoro *et al.*, and which is due to the electrostatic ambipolar field.[21] For our conditions, one would expect that $\mathbf{F}_{sh}$ is only significant in the presheath (about 1 cm from walls for the base case) where the gradient of the plasma potential and B_{rf} are largest. $\mathbf{F}_{sh}$ likely affects, on a fractional basis, low-energy electrons most severely as the high-energy electrons quickly transverse through the presheath. Since inclusion of B_{rf} affects the Legendre coefficients at high energies most severely, as shown in Fig. 7, one might conclude that the angular anisotropy of AEEDs is not particularly sensitive to $\mathbf{F}_{sh}$.

Noncollisional heating, nonlinear electron dynamics, and warm plasma effects are significant at low pressure, when the skin layer is anomalous, and are weak at high pressure, when the collision frequency is large.[9,14,18] Consequently, the Legendre coefficients change significantly with pressure, as shown in Fig. 8. At 1 mTorr, when the NLF and warm plasma effects are important, a_3 in the rz plane is large at high energies, implying there is anisotropy in the AEEDs in the $-v_z$ direction. The coefficients at 50 mTorr, when the collision frequency is large, are an order of magnitude smaller than a_0, implying a more isotropic distribution. Note that the coefficients slowly decrease with energy at 1 mTorr, whereas those at 50 mTorr exponentially decrease as their energy increases. These trends can be explained by the different mechanisms for electron heating at 1 and 50 mTorr. At 50 mTorr, the electrons are highly collisional and Ohmic heating dominates, which yields electron distributions with a low-energy tail. At 1 mTorr, collisionless heating dominates over Ohmic heating and forms EEDs with a high-energy tail.[25,26]

The even coefficients in the θr plane are large at both 1 and 50 mTorr, implying that there is anisotropy in the AEEDs over a wide range of pressures originating from both $F_\theta^{(1)}$ and $F_\theta^{(3)}$. The even coefficients at 1 mTorr are larger than those at 50 mTorr, as the nonlinear force $F_\theta^{(3)}$, acting on the high-energy electrons, is larger at low pressures and weaker at high pressures. In contrast, the odd coefficients increase with pressure as they originated from the collisions, which randomize the purely harmonic electron oscillations and produce the phase difference between v_θ and E_θ.

IV. CONCLUDING REMARKS

The anisotropy of AEEDs in low-pressure ICPs was investigated using Monte Carlo techniques by sampling the trajectories of the electrons and computing Legendre coefficients. The AEED is anisotropic in the rz plane, favoring the high-order odd coefficients. The $-v_z$ component dominates at low frequencies and pressures due largely to the nonlinear Lorentz forces. The anisotropy is largest at higher energies. In the θr plane, even coefficients dominate, implying a large w_θ drift velocity in the azimuthal electric field. We found that the anisotropy in the θr plane is due to electron acceleration by linear electrodynamic and nonlinear third-order forces. Anisotropy in the rz plane dominantly occurs when the skin layer is anomalous, whereas anisotropy in the θr plane persists to higher pressures. For operating conditions typical of plasma processing reactors, higher Legendre coefficients in both the rz and θr planes have significant values.

ACKNOWLEDGMENTS

This work was supported by the CFD Research Corporation, the Semiconductor Research Corporation, and the National Science Foundation (Grant CTS99-74962).

[1] Z. L. Petrovic and T. Makabe, Mater. Sci. Forum **282–283**, 47 (1998).
[2] D. J. Economou, Thin Solid Films **365**, 348 (2000).
[3] U. Kortshagen, A. Maresca, K. Orlov, and B. Heil, Appl. Surf. Sci. **192**, 244 (2002).
[4] J. T. Dakin, IEEE Trans. Plasma Sci. **19**, 991 (1991).
[5] O. Popov and J. Maya, Plasma Sources Sci. Technol. **9**, 227 (2000).
[6] L. Delzeit, I. McAninch, B. A. Cruden, D. Hash, B. Chen, J. Han, and M. Meyyappan, J. Appl. Phys. **91**, 6027 (2002).
[7] V. A. Godyak and R. B. Piejak, Phys. Rev. Lett. **65**, 996 (1990).
[8] V. I. Kolobov and W. N. G. Hitchon, Phys. Rev. E **52**, 972 (1995).
[9] V. A. Godyak, B. M. Alexandrovich, and V. I. Kolobov, Phys. Rev. E **64**, 026406 (2001).
[10] A. V. Vasenkov and M. J. Kushner, Phys. Rev. E **66**, 066411 (2002).
[11] V. I. Kolobov and D. J. Economou, Plasma Sources Sci. Technol. **6**, R1 (1997).
[12] R. C. Woods and I. D. Sudit, Phys. Rev. E **50**, 2222 (1994).
[13] A. J. Christlieb, W. N. G. Hitchon, and E. R. Keiter, IEEE Trans. Plasma Sci. **28**, 2214 (2000).
[14] Y. O. Tyshetskiy, A. Smolyakov, and V. Godyak, Plasma Sources Sci. Technol. **11**, 203 (2002).
[15] L. C. Pitchford and A. V. Phelps, Phys. Rev. A **25**, 540 (1982).
[16] J. A. Meyer, R. Mau, and A. E. Wendt, J. Appl. Phys. **79**, 1298 (1996).
[17] V. I. Kolobov, D. P. Lymberopoulos, and D. J. Economou, Phys. Rev. E **55**, 3408 (1997).
[18] V. A. Godyak, Bulgarian J. Phys. **27**, 1 (2000).
[19] A. Sankaran and M. J. Kushner, J. Appl. Phys. **92**, 736 (2002).
[20] T. E. F. M. Standaert, M. Schaepkens, N. R. Rueger, P. G. M. Sebel, G. S. Oehrlein, and J. M. Cook, J. Vac. Sci. Technol. A **16**, 239 (1998).
[21] M. Tasokoro, H. Hirata, N. Nakano, Z. L. Petrovic, and T. Makabe, Phys. Rev. E **57**, R43 (1998).
[22] M. A. Lieberman and A. J. Lichtenberg, *Principles of Plasma Discharges and Materials Processing* (Wiley, New York, 1994).
[23] R. B. Piejak and V. A. Godyak, Appl. Phys. Lett. **76**, 2188 (2000).
[24] F. F. Chen, Phys. Plasmas **8**, 3008 (2001).
[25] S. Rauf and M. J. Kushner, J. Appl. Phys. **81**, 5966 (1997).
[26] V. A. Godyak, R. B. Piejak, and B. M. Alexandrovich, Plasma Sources Sci. Technol. **3**, 169 (1994).